forests

MDPI

Article

Analysis and Tests of Lateral Resistance of Bolted and Screwed Connections of CLT

Liangliang Huo [1], Enchun Zhu [2,*], Shuang Niu [2] and Guofang Wu [3]

[1] School of Civil Engineering/Key Lab of Structures Dynamic Behavior and Control of China Ministry of Education, Harbin Institute of Technology, Harbin 150090, China; 1123310614@hit.edu.cn
[2] Department of Civil Engineering, School of Ocean Engineering, Harbin Institute of Technology at Weihai, Weihai 264209, China; nius@hit.edu.cn
[3] Research Institute of Wood Industry, China Academy of Forestry, Beijing 100091, China; gfwu@caf.ac.cn
* Correspondence: e.c.zhu@hit.edu.cn

Abstract: The lateral resistance of dowel-type connections with CLT is related to its lay-up, species of the laminations and even the manufacture method. Treating the CLT as homogeneous material, current methods develop new equations through test results or make use of the existing equations for the embedment strength already used in design codes; thus, the lateral resistance of dowel-type connections of CLT can be calculated. This kind of approach does not take the embedment stress distribution into account, which may lead to inaccuracy in predicting the lateral resistance and yield mode of the dowel-type connections in CLT. In this study, tests of the bolted connections and the screwed connections of CLT were conducted by considering the effects of the orientation of the laminations, the thickness of the connected members, the fastener diameter and strength of the materials. The material properties including yield strength of the fasteners and embedment strength of the CLT laminations were also tested. Using analysis of the dowel-type connections of CLT by introducing the equivalent embedment stress distribution, equations for the lateral resistance of the connections based on the European Yield Model were developed. The predicted lateral resistance and yield modes were in good agreement with the test results; the correctness and the feasibility of the equations were thus validated.

Keywords: cross-laminated timber; lateral resistance; European Yield Model; bolted connection; screwed connection; embedment stress

check for updates

Citation: Huo, L.; Zhu, E.; Niu, S.; Wu, G. Analysis and Tests of Lateral Resistance of Bolted and Screwed Connections of CLT. *Forests* **2022**, *13*, 375. https://doi.org/10.3390/f13030375

Academic Editors: Barbara Ozarska and Angela Lo Monaco

Received: 1 January 2022
Accepted: 21 February 2022
Published: 23 February 2022

Publisher's Note: MDPI stays neutral with regard to jurisdictional claims in published maps and institutional affiliations.

Copyright: © 2022 by the authors. Licensee MDPI, Basel, Switzerland. This article is an open access article distributed under the terms and conditions of the Creative Commons Attribution (CC BY) license (https://creativecommons.org/licenses/by/4.0/).

1. Introduction

Being naturally grown and environmentally friendly, timber has become more and more popular as a green building material. Research and development of wood products have been growing fast [1,2]. The relatively high in-plane stiffness and dimension stability along with the need of green building materials make CLT an alternative to concrete and steel [3]. At present, a lot of experimental and numerical research on material properties of CLT and CLT members is being conducted [4–8]. Bolted or screwed connections play a vital role of providing resistance, stiffness and ductility for CLT buildings [9,10]. Experimental investigations showed that the primary damage of CLT buildings subjected to lateral load is concentrated on the connections [11–13]. Calculations of the lateral resistance of such dowel-type connections of CLT are, therefore, fundamental to the design of the CLT buildings. According to the European Yield Model (EYM) [14], a fastener is assumed as a beam loaded by the embedment stress due to interactions between the fastener and wood. The embedment stress at yield of wood is defined as the embedment strength, which is related to the wood density, the fastener diameter and the grain orientation [15,16]. The lateral resistance of a dowel-type connection can be predicted with the embedment strength of the connected members and the yield moment of fasteners [17]. However, with CLT, the embedment strength of the longitudinal and transverse laminations may differ from each

other, and different combinations of the laminations and species of wood may make the calculations of the lateral resistance of dowel-type connections of CLT more complicated, making it a major challenge to design of the structures.

The lateral resistance of dowel-type connections of CLT is still calculated in accordance with the EYM, yet different methods are employed to determine the embedment strength of CLT. It seems that methods for determining the embedment strength of CLT can be classified into two broad types—either to develop new equations specially for CLT or to modify the existing equations for wood to suit CLT. In developing the new equations, extensive experimental investigations of the embedment strength of CLT and the lateral resistance of the connections have been conducted [18]. Uibel and Blaß [19,20] conducted embedment tests of three-layer and five-layer CLT made of European Spruce (*Picea abies*), with the smooth dowels positioned perpendicular to the wide face and the narrow sides of CLT panels, respectively. They then developed empirical equations for the embedment strength of CLT in relation to the density of wood and diameter of dowels via regression of the test results. The equations are adopted in the technical manuals of some European countries [21,22]. However, a difference up to 22% can be found between the test results conducted by Tuhkanen et al. [23] and the empirical equations proposed by Uibel and Blaß [19]. The empirical equations were also found to yield higher predictions for screwed wood-to-CLT connections [24]. Kennedy et al. [25] conducted embedment tests of Canadian made CLT with lag screws and self-drilling screws positioned perpendicular to the wide face. The equations for the embedment strength of CLT were derived from regression of their test results. The predictions with the empirical equations proposed by Kennedy et al. [25] were found to be 40% lower on average than those proposed by Uibel and Blaß [19].

In another type of method, making use of the equations for the embedment strength of wood already adopted in design codes, either the embedment strength of wood or the thickness of the CLT laminations is modified first, and then the lateral resistance of the dowel-type connections of CLT is calculated using the current equations following the EYM. In the newly revised CSA O86 [26], the equations for embedment strength and lateral resistance applicable to all other wood products are retained, and an adjustment factor of 0.9 to discount the embedment strength of CLT is introduced, in consideration of the possibility for a fastener to be installed over a gap or unglued edges between the laminations. In NDS [27], the embedment strength of the lamination at the shear plane is taken as the nominal embedment strength of CLT. If the lamination is loaded parallel to grain, thickness of the perpendicular laminations will be adjusted by a ratio of the embedment strength perpendicular to grain to that parallel to grain, taking into account the weaker transverse laminations. This way, the resultant of the embedment stress can be calculated correctly, yet the bending moment on the dowel cannot be correct, since the length of stress distribution is modified by discounting the thickness of the perpendicular laminations. This treatment may cause errors in calculating the lateral resistance and in determining the yield mode of the connections. Scoichi et al. [28] calculated the embedment strength of the longitudinal laminations using the conventional equations for wood. Assuming that the embedment strength of the transverse laminations is half of the longitudinal laminations and the thickness of each layer of laminations is the same, they then derived equations for lateral resistance of drift pin connections in five-layer CLT. Mahdavifar et al. [29] conducted a test and analysis of nailed and screwed connections of hybrid CLT (layers made of different species or grades of laminations) with a steel side plate. Their analysis, making use of the embedment strength of the laminations, was only applicable to the situation where the fastener penetrated just two layers of laminations. Further studies are still needed to determine the lateral resistance of dowel-type connections in CLT.

In this study, tests of double shear bolted timber-to-CLT connections and tests of single shear screwed steel-to-CLT connections were conducted. Different grain orientations, thicknesses of the connected members and diameters of bolts and screws in relation to different yield modes were considered. As part of the experimental investigations, material

properties including yield strength of the fasteners and embedment strength of the laminations were also tested or measured. The bolted and screwed connections of CLT were analyzed by employing the equivalent embedment stress distribution. The equations for the lateral resistance of the connections were developed in conjunction with the analysis. The test results and the analytical predictions correlated closely, the proposed equations and method were thus validated and a method for calculating the lateral resistance was provided.

2. Materials and Methods

2.1. Materials

2.1.1. Specimens to Test the Material Properties

High-strength bolts of Grade 8.8 [30] and self-tapping screws were used in this study. Bolts with the effective diameter of 10.6 mm, 12.6 mm and 14.6 mm, corresponding to the thread diameter of 12.0 mm, 14.0 mm and 16.0 mm, respectively, were used in tests of the bolted connections. To determine the yield strength of the bolts, the bolt specimens with a length of 300 mm were tested. The bolt specimens as shown in Figure 1a were divided into 3 groups according to the thread diameter. Screws with the effective diameter of 5.0 mm and 10.0 mm, corresponding to the thread diameter of 7.5 mm and 12.0 mm, respectively, were used in tests of the screwed connections. To determine the yield strength of the screws, the screw specimens with a length of 100 mm were tested. The screw specimens as shown in Figure 1b were divided into 2 groups according to the effective diameter. The details of the bolt specimens and screw specimens are listed in Table 1.



(**a**) (**b**)

Figure 1. Photos of the fastener specimens. (**a**) Bolt specimens and (**b**) screw specimens.

Table 1. Group and geometry of the fastener specimens.

Group	Type	Thread Diameter (mm)	Effective Diameter (mm)	Length (mm)
D12 *	Bolt of Grade 8.8	12.0	10.6	300
D14	Bolt of Grade 8.8	14.0	12.6	300
D16	Bolt of Grade 8.8	16.0	14.6	300
D5	Self-Tapping Screws	7.5	5.0	100
D10	Self-Tapping Screws	12.0	10.0	100

* D indicates diameter of the fastener specimens.

In accordance with ASTM D 5764 [31], half-hole embedment tests were conducted to evaluate the embedment strength of the Hemlock (*Tsuga heterophylla*) laminations of CLT. The embedment test specimens with a half bolt hole were 100 mm long, 100 mm wide and 33 mm thick, which were large enough to prevent splitting. In total, 288 specimens were

used for the bolt embedment test and 192 specimens were used for the screw embedment test. The specimens for the bolt embedment test were divided into 6 groups, with 48 in each group in accordance with bolt diameter and orientation of lamination of CLT. The specimens for the screw embedment test were divided into 4 groups, also with 48 in each group in accordance with screw diameter and orientation of lamination of CLT.

2.1.2. Bolted Connection Specimens

The details of a double shear bolted timber-to-CLT connection specimen are shown in Figure 2. The main member with a thickness of 105 mm was the three-layer CLT made of Hemlock dimension lumber of Grade No. 1 [26]. The side members were Scotch Pine (*Pinus sylvestris* L. var. *mongolica* Litv.) sawn timber of Grade TC 11 [32], with thicknesses of 10 mm, 40 mm and 70 mm, respectively. The bolts were of Grade 8.8 [30] with diameters of 12 mm, 14 mm and 16 mm, respectively. Corresponding to the bolt diameter, dimensions (length × width) of the connected members were 150 mm × 80 mm, 180 mm × 90 mm and 200 mm × 100 mm, respectively. According to ASTM D 5652 [33], the bolt hole was 1.6 mm wider than the bolt diameter. As listed in Table 2, 90 specimens were divided into 18 groups according to the bolt diameter and thickness of the side members, with each group containing 5 specimens. In addition, 9 groups of the specimens were loaded parallel to grain of the surface lamination of the CLT, and the other 9 groups were loaded perpendicular to grain of the surface lamination of the CLT.

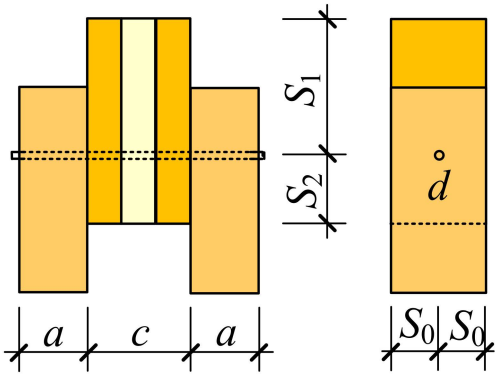


Figure 2. Schematic of a bolted connection specimen.

Table 2. Details of the double shear bolted timber-to-CLT connection specimens.

Longitudinal Direction						Transverse Direction					
Group	**Diameter d (mm)**	**a [1] (mm)**	**S_0 [2] (mm)**	**S_1 [3] (mm)**	**S_2 [4] (mm)**	**Group**	**Diameter d (mm)**	**a (mm)**	**S_0 (mm)**	**S_1 (mm)**	**S_2 [5] (mm)**
B1 [5]	12	10	40	100	50	B10	12	10	40	100	50
B2	14	10	45	120	60	B11	14	10	45	120	60
B3	16	10	50	130	70	B12	16	10	50	130	70
B4	12	40	40	100	50	B13	12	40	40	100	50
B5	14	40	45	120	60	B14	14	40	45	120	60
B6	16	40	50	130	70	B15	16	40	50	130	70
B7	12	70	40	100	50	B16	12	70	40	100	50
B8	14	70	45	120	60	B17	14	70	45	120	60
B9	16	70	50	130	70	B18	16	70	50	130	70

[1] a is the thickness of the side member; [2] S_0 is the edge distance; [3] S_1 is the end distance loaded; [4] S_2 is the end distance unloaded; [5] B indicates bolted timber-to-CLT connection specimens.

2.1.3. Screwed Connection Specimens

Figure 3 shows the details of a single shear screwed steel-to-CLT connection specimen. The steel plate was of Grade Q235 [30], with thicknesses of 4 mm and 6 mm, respectively.

The diameters of the self-tapping screws were 5 mm and 10 mm, respectively. As listed in Table 3, there were 40 specimens, which were divided into 8 groups, with 5 in each group in accordance with the screw diameter, steel plate thickness and orientation of the CLT member.

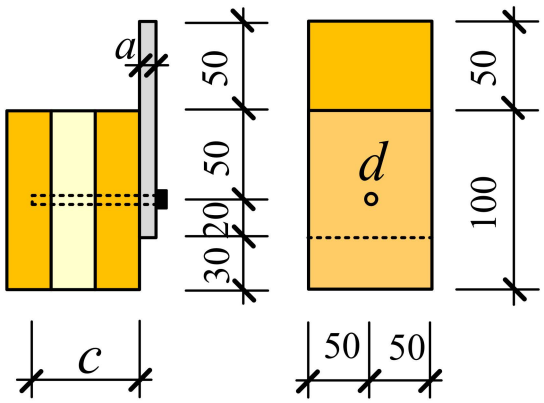


Figure 3. Schematic of a screwed connection specimen.

Table 3. Details of the single shear screwed steel-to-CLT connection specimens.

Longitudinal Direction			Transverse Direction		
Group	**Diameter *d* (mm)**	**Steel Plate Thickness *a* (mm)**	**Group**	**Diameter *d* (mm)**	**Steel Plate Thickness *a* (mm)**
S1 *	5	4	S5	5	4
S2	10	4	S6	10	4
S3	5	6	S7	5	6
S4	10	6	S8	10	6

* S indicates screwed steel-to-CLT connection specimens.

2.2. Methods

As shown in Figure 4, tension tests were conducted at a loading rate of 0.2 mm/min to determine the yield strength of the bolts in accordance with ASTM A 370 [34] and the yield strength of the screws in accordance with ASTM F 606 [35].



Figure 4. Tension test of bolts.

In accordance with ASTM D 5764 [31], tests were conducted for the embedment strength of the CLT laminations. As shown in Figure 5, a compression load was applied to the specimen at a rate of 1 mm/min. A load cell was applied to measure the load. Two linear variable differential transducers (LVDT's) were symmetrically arranged to measure

the deformation. As shown in Figure 6, the embedment strength was derived from the load–deformation curves. The initial linear portion of the curve offset 5% of the fastener diameter. If the offset line intersected the load–deformation curve, the load at the intersection was taken as the yield load, otherwise the maximum load was taken as the yield load. The embedment strength was determined by dividing the yield load by the thickness of the specimen and the fastener diameter. After testing, the specific gravity and the moisture content of the specimen were measured in accordance with ASTM D 2395 [36] and ASTM D 4442 [37], respectively.



Figure 5. Test for embedment strength of the laminations.

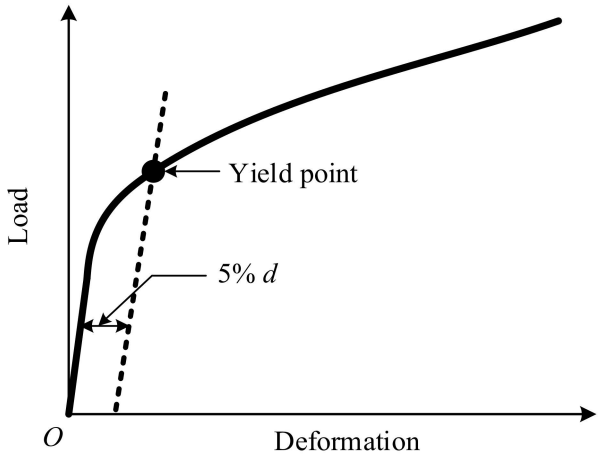


Figure 6. The 5%*d* offset method for the yield load.

As shown in Figure 7, tests were conducted with a computer-controlled electronic universal testing machine applying a compression load at a rate of 1 mm/min. The load was measured with a load cell, and the relative displacement between the connected members was measured with two symmetrically arranged LVDT's. The load continued to increase until the relative displacement of 15 mm or the maximum load was reached according to ASTM D 5652 [33].



(**a**) (**b**)

Figure 7. Setup for test of the bolted connections. (**a**) Front view and (**b**) side view.

As shown in Figure 8, the screwed connection specimen was anchored to the testing machine with a piece of steel angle, and the compression load was applied at a rate of 1 mm/min. The load was measured with a load cell, and the relative displacement between the CLT member and the steel plate was measured with a LVDT.



Figure 8. Setup for test of the screwed connections.

2.3. Analysis of the Lateral Resistancce

2.3.1. Yield Mode

According to the EYM, a dowel-type connection fails when the embedment stress reaches the strength of wood or when the dowel yields, provided that sufficient spacing is guaranteed [38]. The yield modes of dowel-type connections in CLT, which are also referred to as the failure modes, are shown in Figure 9.

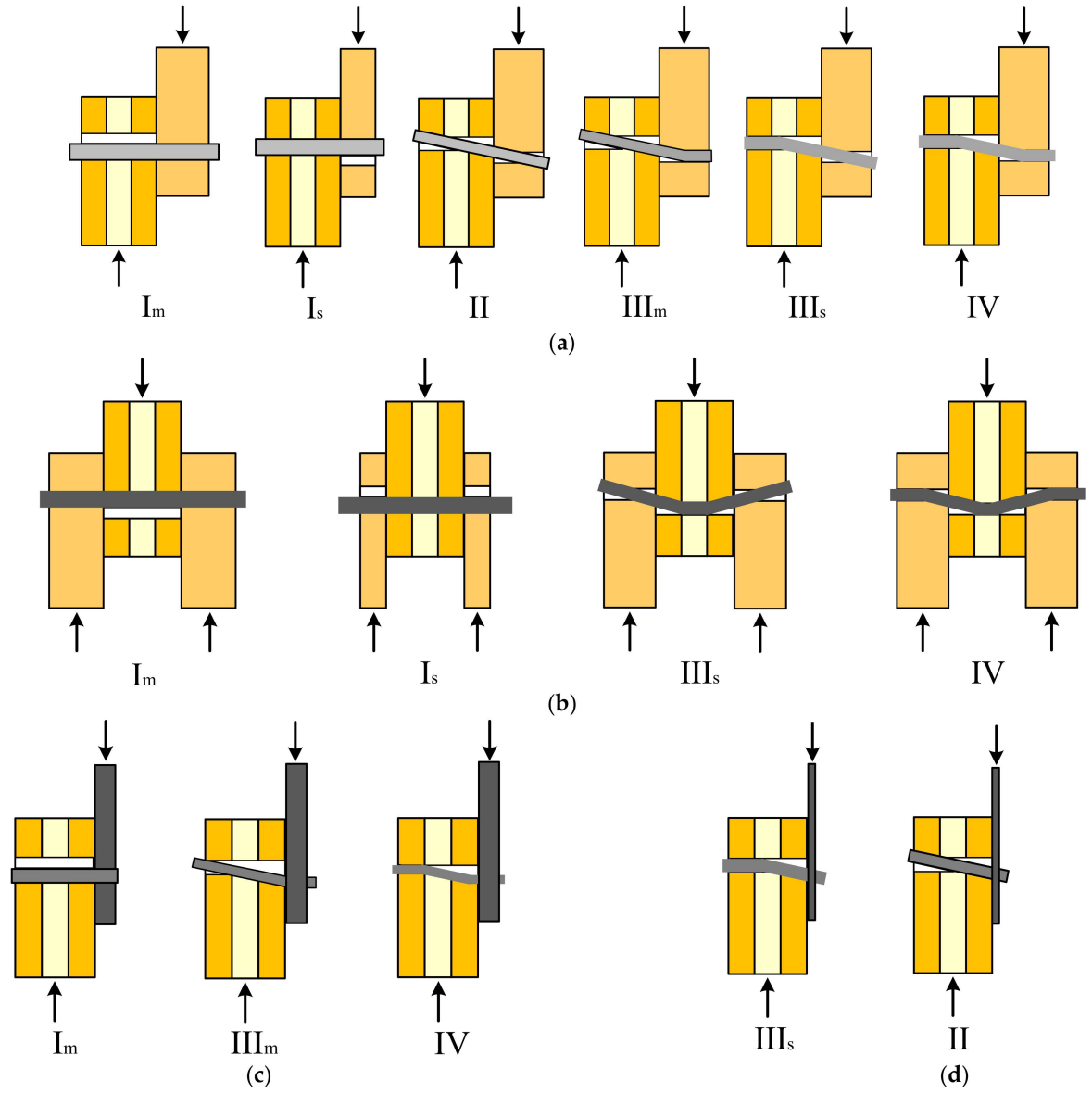


Figure 9. Yield modes for connections of CLT: (**a**) single shear timber-to-CLT connections, (**b**) double shear timber-to-CLT connections, (**c**) steel-to-CLT connections with thick steel plates and (**d**) steel-to-CLT connections with thin steel plates.

2.3.2. Bolted Timber-to-CLT Connections

For a bolted timber-to-CLT connection, the CLT member can be considered as the main member and the timber member as the side member. Following the EYM, the equations for calculating the lateral resistance can be derived as follows.

Single Shear Connections

(1) Yield Mode I_m

The embedment stress distribution is shown in Figure 10, where wood of the CLT member yields along the bolt hole and wood of the side member remains elastic. Lateral resistance R_{Im} is expressed as

$$R_{Im} = \alpha a d f_{h,CLT} = c d f_{h,CLT} \quad (1)$$

$$f_{h,\mathrm{CLT}} = \sum_{i=1}^{n} (t_i f_{\mathrm{hc},i} / c) \tag{2}$$

where α is the ratio of thickness of the CLT member to that of the side member, $\alpha = c/a$; c is thickness of the CLT member; a is thickness of the side member; d is the diameter of the bolt; $f_{\mathrm{h,CLT}}$ is equivalent embedment strength of the CLT member; n is the number of layers of laminations; t_i is the thickness of the ith layer lamination; and $f_{\mathrm{hc},i}$ is the embedment strength of the ith layer lamination.

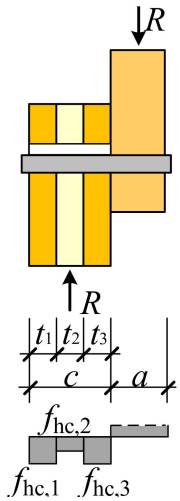


Figure 10. Embedment stress distribution for Yield Mode $\mathrm{I_m}$.

(2) Yield Mode $\mathrm{I_s}$

The embedment stress distribution is shown in Figure 11, where wood of the side member yields along the bolt hole and wood of the CLT member remains elastic. Lateral resistance R_{Is} is expressed as

$$R_{\mathrm{Is}} = adf_{\mathrm{ha}} \tag{3}$$

where f_{ha} is embedment strength of the side member.

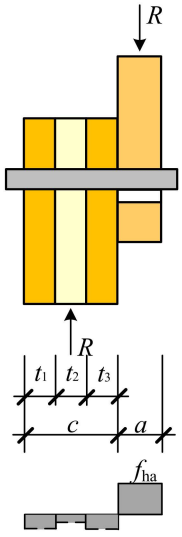


Figure 11. Embedment stress distribution for Yield Mode $\mathrm{I_s}$.

(3) Yield Mode II

As shown in Figure 12, the bolt remains straight in both members. There is a reversal point of the embedment stress distribution in the CLT member, which is considered the reference point of the embedment stress distribution in this study. The reference point can be located in any of the three layers of lamination, which defines different stress distribution in CLT. The lateral resistance could be derived using the direct embedment stress distribution, yet the expressions so derived would be very complex to use. To simplify the situation, a method to calculate the lateral resistance via the equivalent embedment stress distribution is proposed in this study. The equivalent embedment stress distribution for Yield Mode II is shown in Figure 12, where different embedment stress in different layers is represented by the uniformly distributed stress, equaling the embedment strength of the jth layer, in which the reference point is located. The equivalence is realized by introducing an additional shear $F_{\mathrm{II},j}$ and an additional bending moment $M_{\mathrm{II},j}$ to the cross-section of bolt at the interface between the connected members, so that the shear and the bending moment at the interface remain the same before and after making the equivalence. The embedment strength of the lamination containing the reference point $f_{\mathrm{hc},j}$ is taken as the equivalent embedment strength $f_{\mathrm{h,CLT}}$ of the CLT. The additional shear $F_{\mathrm{II},j}$ and bending moment $M_{\mathrm{II},j}$ are derived, respectively, as follows.

$$F_{\mathrm{II},j} = -\sum_{i=1}^{j-1}[t_i d(f_{\mathrm{h,CLT}} - f_{\mathrm{hc},i})] + \sum_{i=j+1}^{n}[t_i d(f_{\mathrm{h,CLT}} - f_{\mathrm{hc},i})] \tag{4}$$

$$M_{\mathrm{II},j} = -\sum_{i=1}^{j-1}\left[\left(t_i/2 + \sum_{k=i+1}^{n} t_k\right) t_i d(f_{\mathrm{h,CLT}} - f_{\mathrm{hc},i})\right] + \sum_{i=j+1}^{n}\left[\left(t_i/2 + \sum_{k=i+1}^{n} t_k\right) t_i d(f_{\mathrm{h,CLT}} - f_{\mathrm{hc},i})\right] \tag{5}$$

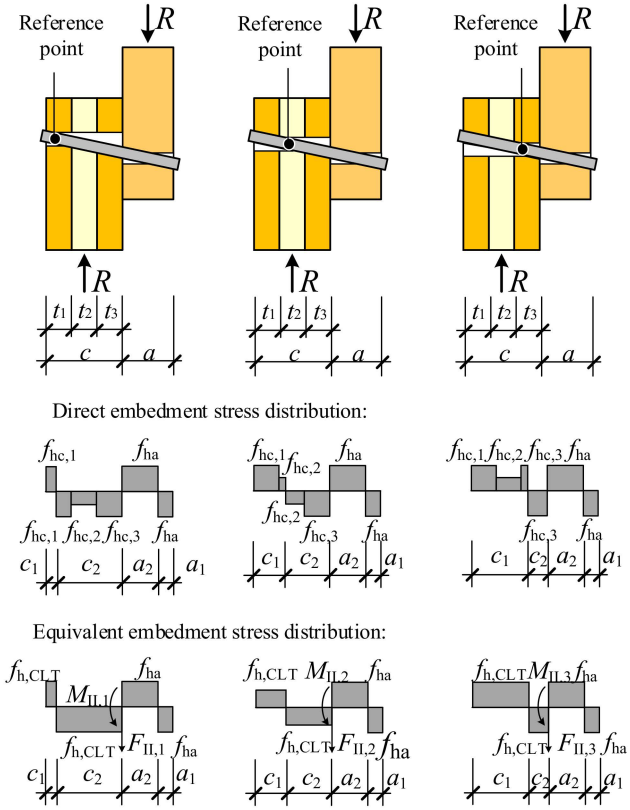


Figure 12. Embedment stress distribution for Yield Mode II (three-layer CLT).

Using the equivalent stress distribution, the vertical equilibrium and the moment equilibrium of the bolt at the interface of the connected members are as follows.

$$R_{\mathrm{II},j} = (a_2 - a_1) d f_{\mathrm{ha}} = (c_2 - c_1) d f_{\mathrm{h,CLT}} - F_{\mathrm{II},j} \tag{6}$$

$$f_{\mathrm{ha}} d (a_2 - a_1)^2/2 - f_{\mathrm{ha}} d {a_1}^2 + f_{\mathrm{h,CLT}} d (c_2 - c_1)^2/2 - f_{\mathrm{h,CLT}} d {c_1}^2 - M_{\mathrm{II},j} = 0 \tag{7}$$

The lateral resistance for Yield Mode II can be derived as

$$R_{\mathrm{II},j} = \frac{a d f_{\mathrm{ha}}}{\beta + 1} \left[\sqrt{\beta + 2\beta^2 (1 + \alpha + \alpha^2) + \alpha^2 \beta^3 + \omega_{\mathrm{III}_m,j}} - \beta (1 + \alpha) \right] \tag{8}$$

$$\omega_{\mathrm{II},j} = \frac{2(1+\beta) F_{\mathrm{II},j}}{a d f_{ha}} \left(F_{\mathrm{II},j} \alpha \beta + \frac{2\beta M_{\mathrm{II},j}}{a} - \frac{F_{\mathrm{II},j}^2}{2 a d f_{\mathrm{ha}}} \right) \tag{9}$$

where β is the ratio of the equivalent embedment strength of the CLT member to the embedment strength of the side member, $\beta = f_{\mathrm{h,CLT}}/f_{\mathrm{ha}}$; $\omega_{\mathrm{II},j}$ is an item supplementary to the ordinary expression for timber-to-timber connections and is related to the additional shear and bending moment due to the equivalence.

(4) Yield Mode $\mathrm{III_m}$

As shown in Figure 13, the bolt remains straight in the CLT member, and a plastic hinge is formed in the side member. Following the principle of the equivalence, the lateral resistance $R_{\mathrm{IIIm},j}$ for Yield Mode $\mathrm{III_m}$ with the reference point being located in the jth layer lamination can be derived as

$$R_{\mathrm{IIIm},j} = \frac{a a d f_{\mathrm{ha}}}{2\beta + 1} \left[\sqrt{2\beta^2 (1 + \beta) + \frac{4\beta (2\beta + 1) M_y}{(a a)^2 d f_{\mathrm{ha}}} + w_{\mathrm{IIIm},j}} - \left(\beta + \frac{F_{\mathrm{IIIm},j}}{a a d f_{\mathrm{ha}}} \right) \right] \tag{10}$$

$$\omega_{\mathrm{IIIm},j} = \frac{4\beta (1 + 2\beta) M_{\mathrm{IIIm},j}}{(\alpha a)^2 d f_{\mathrm{ha}}} - \frac{2\beta F_{\mathrm{IIIm},j}}{\alpha a d f_{\mathrm{ha}}} \left(2\beta + \frac{F_{\mathrm{IIIm},j}}{\alpha a d f_{\mathrm{ha}}} \right) \tag{11}$$

$$F_{\mathrm{IIIm},j} = -\sum_{i=1}^{j-1} [t_i d (f_{\mathrm{h,CLT}} - f_{\mathrm{hc},i})] + \sum_{i=j+1}^{n} [t_i d (f_{\mathrm{h,CLT}} - f_{\mathrm{hc},i})] \tag{12}$$

$$M_{\mathrm{IIIm},j} = -\sum_{i=1}^{j-1} \left[\left(\frac{t_i}{2} + \sum_{k=i+1}^{n} t_k \right) t_i d (f_{\mathrm{h,CLT}} - f_{\mathrm{hc},i}) \right] + \sum_{i=j+1}^{n} \left[\left(\frac{t_i}{2} + \sum_{k=i+1}^{n} t_k \right) t_i d (f_{\mathrm{h,CLT}} - f_{\mathrm{hc},i}) \right] \tag{13}$$

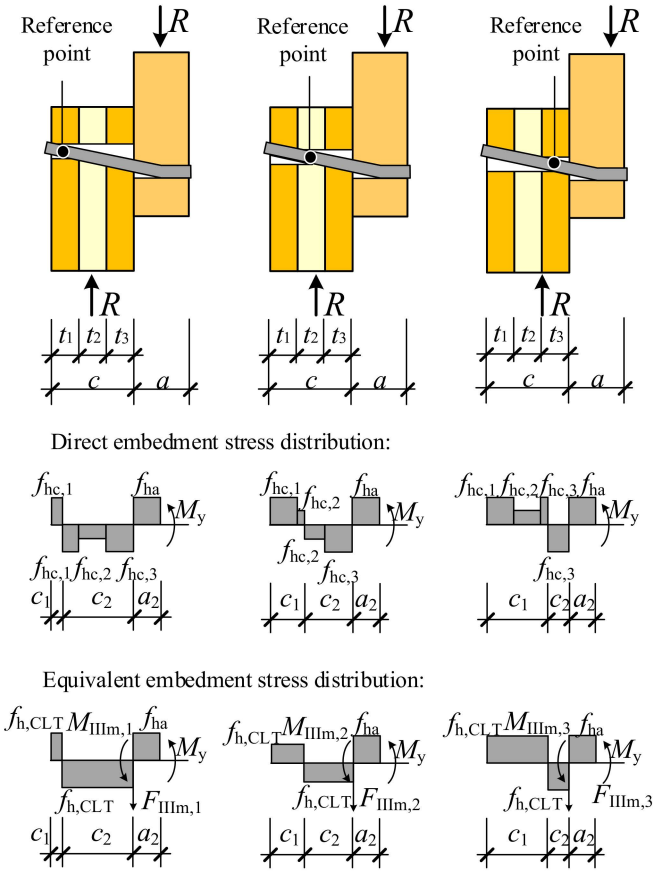


Figure 13. Embedment stress distribution for Yield Mode III_m (three-layer CLT).

(5) Yield Mode III_s

As shown in Figure 14, a plastic hinge of the bolt is formed in the CLT member, and the bolt remains straight in the side member. The embedment strength of the *j*th layer lamination containing the plastic hinge is taken as the equivalent embedment strength of the CLT.

By simplifying the embedment stress distribution with the equivalent distribution, the lateral resistance $R_{IIIs,j}$ for Yield Mode III_s can be derived as

$$R_{IIIs,j} = \frac{adf_{ha}}{2+\beta}\left[\sqrt{2\beta(\beta+1)+\frac{4\beta(2+\beta)M_y}{a^2df_{ha}}+\omega_{IIIs,j}}-\left(\beta+\frac{2F_{IIIs,j}}{adf_{ha}}\right)\right] \quad (14)$$

$$\omega_{IIIs,j} = \left(2-\frac{F_{IIIs,j}}{adf_{ha}}\right)\frac{2\beta F_{IIIs,j}}{adf_{ha}}+\frac{4\beta(2+\beta)M_{IIIs,j}}{a^2df_{ha}} \quad (15)$$

$$F_{IIIs,j} = \sum_{i=j+1}^{n}\left[t_i d(f_{h,CLT}-f_{hc,i})\right] \quad (16)$$

$$M_{IIIs,j} = \sum_{i=j+1}^{n}\left[\left(\frac{t_i}{2}+\sum_{k=i+1}^{n}t_k\right)t_i d(f_{h,CLT}-f_{hc,i})\right] \quad (17)$$

where *j* is the sequence number of the layer of lamination in which the plastic hinge is located; $F_{IIIs,j}$ and $M_{IIIs,j}$ are, respectively, the additional shear and bending moment of the bolt at the interface of the connected members.

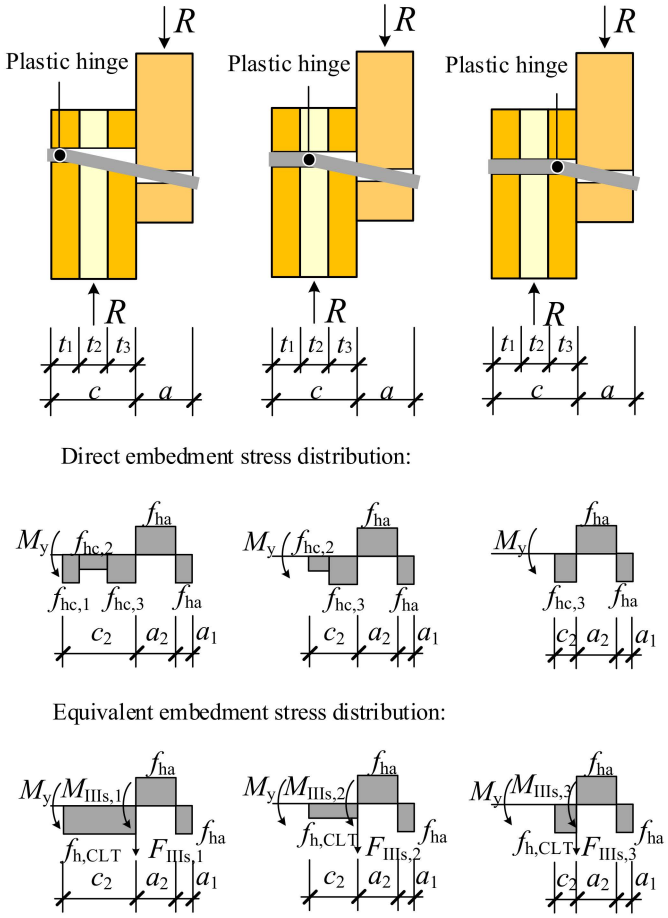


Figure 14. Embedment stress distribution for Yield Mode III_s (three-layer CLT).

(6) Yield Mode IV

As shown in Figure 15, the bolt bends in both members, resulting in two plastic hinges. Following the principle of the equivalence, lateral resistance with a plastic hinge located in the *j*th layer lamination can be derived as

$$R_{IV,j} = daf_{ha}\left[\sqrt{\frac{4\beta My_y}{a^2(\beta+1)df_{ha}} + \omega_{IV,j}} - \frac{F_{IV,j}}{(\beta+1)adf_{ha}}\right] \tag{18}$$

$$\omega_{IV,j} = \frac{2\beta M_{IV,j}}{(\beta+1)a^2df_{ha}} - \frac{\beta F_{IV,j}^2}{(\beta+1)^2a^2d^2f_{ha}^2} \tag{19}$$

$$F_{IV,j} = \sum_{i=j+1}^{n}\left[t_i d(f_{h,CLT} - f_{hc,i})\right] \tag{20}$$

$$M_{IV,j} = \sum_{i=j+1}^{n}\left[\left(\frac{t_i}{2} + \sum_{k=i+1}^{n} t_k\right)t_i d(f_{h,CLT} - f_{hc,i})\right] \tag{21}$$

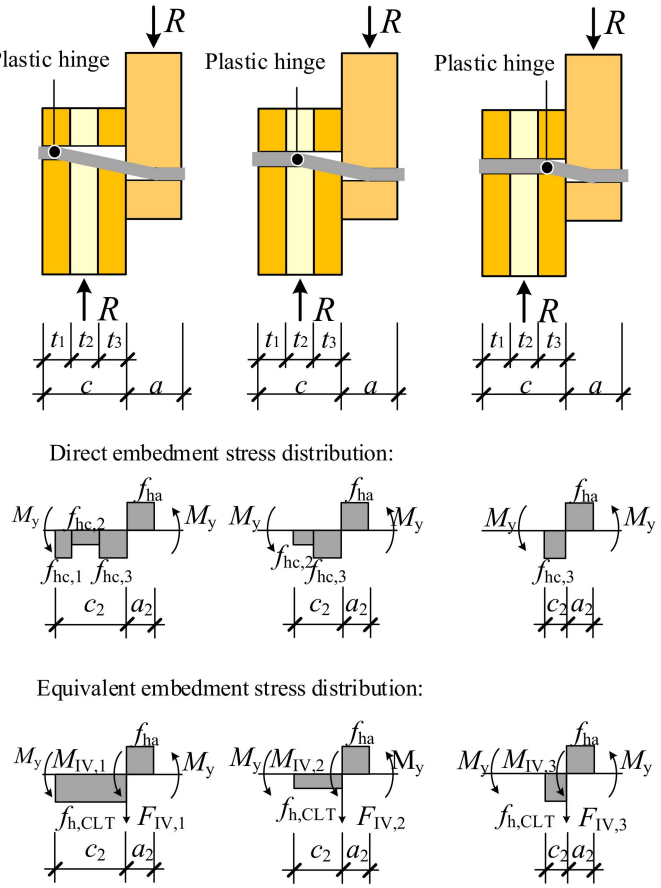


Figure 15. Embedment stress distribution for Yield Mode IV (three-layer CLT).

Double Shear Connection

For a symmetrical double shear bolted connection of CLT, Yield Modes II and III_m are excluded due to the symmetry of bolt deformation. The lateral resistance can be calculated the same way as with a single shear connection, except for Yield Mode I_m, where the half thickness $c/2$ of the CLT member is used to calculate the lateral resistance per shear plane. The lateral resistance per bolt per shear plane of both the single shear and double shear connections is the minimum between all the yield modes, calculated as follows.

$$R = \min\{R_{Im}, R_{Is}, R_{II,j}, R_{IIIm,j}, R_{IIIs,j}, R_{IV,j}\} \quad (22)$$

2.3.3. Bolted Steel-to-CLT Connections

Lateral resistance of a steel-to-CLT connection can be calculated by treating the steel plate as the side member. Due to relatively the small thickness and high embedment strength of the steel plate, calculations of the lateral resistance of steel-to-CLT connections can be simplified as follows.

Thick Steel Plate

For a steel-to-CLT connection, Yield Mode I_s shall not occur if the steel side plate is assumed not to yield. According to Eurocode 5 [39], a steel plate with a thickness not smaller than the dowel diameter is considered as a thick steel plate. If a thick steel side plate is used, only Yield Mode I_m, III_m or IV occurs. Lateral resistance for Mode I_m can

be calculated with Equations (1) and (2). For Yield Mode III_m shown in Figure 16, lateral resistance can be obtained by treating $\beta = f_{h,CLT}/f_{ha} = 0$ in Equation (10), as follows.

$$R_{IIIm,j} = cdf_{h,CLT}\left[\sqrt{\frac{4M_y}{c^2df_{h,CLT}} + 2 + \frac{4M_{IIIm,j}}{c^2df_{h,CLT}}} - \left(1 + \frac{F_{IIIm,j}}{cdf_{h,CLT}}\right)\right] \quad (23)$$

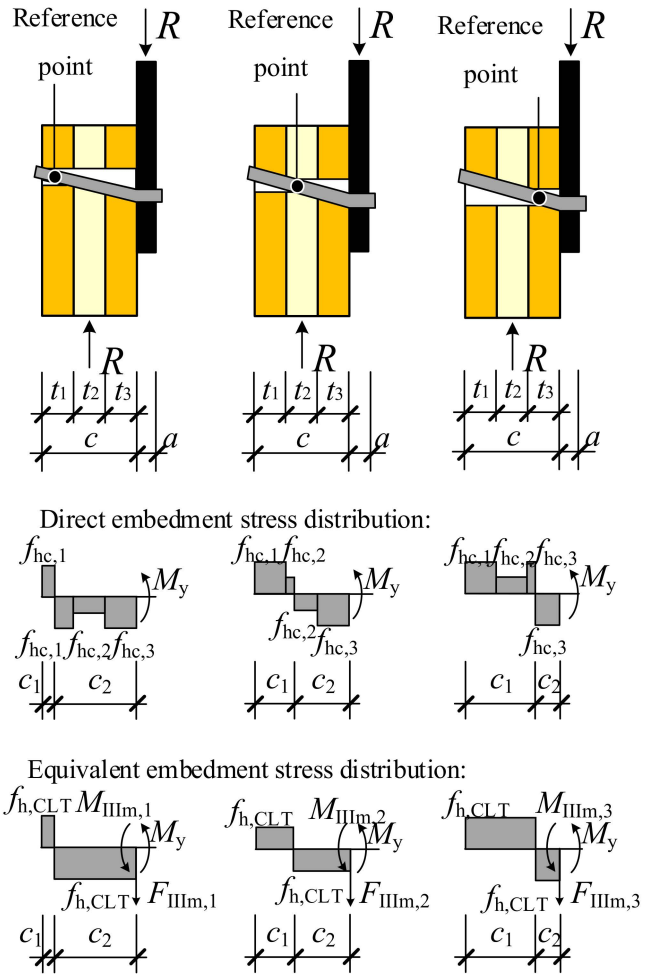


Figure 16. Embedment stress distribution for Yield Mode III_m (three-layer CLT).

For Yield Mode IV of the steel-to-CLT connections shown in Figure 17, lateral resistance can be obtained by treating $\beta = 0$ in Equation (18), as follows.

$$R_{IV,j} = \sqrt{4df_{h,CLT}M_y + 2df_{h,CLT}M_{IV,j}} - F_{IV,j} \quad (24)$$

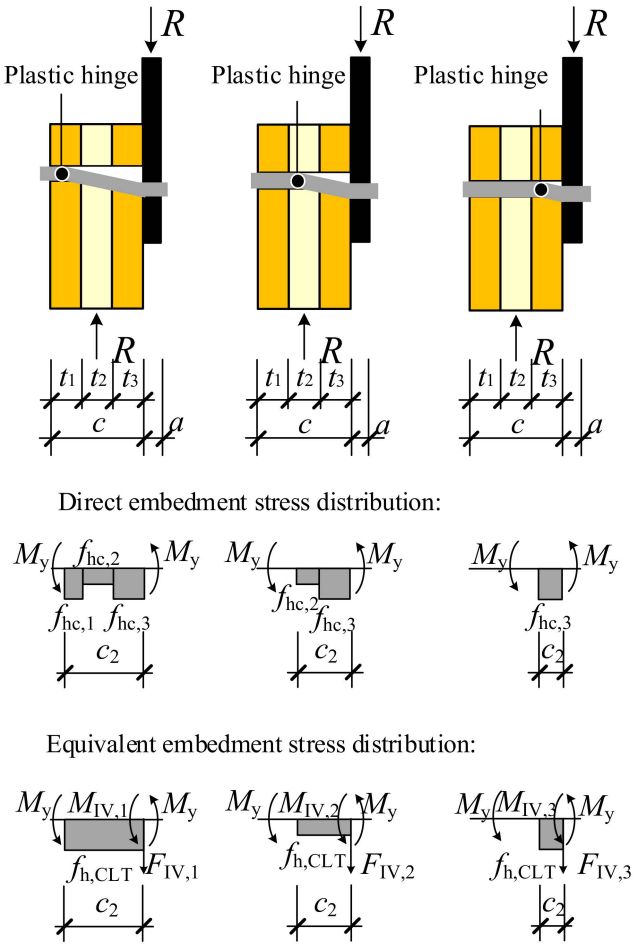


Figure 17. Embedment stress distribution for Yield Mode IV (three-layer CLT).

Lateral resistance of a steel-to-CLT connection with a thick steel side plate is the minimum among the yield modes mentioned above.

$$R = \min\{R_{\mathrm{Im}}, R_{\mathrm{IIIm},j}, R_{\mathrm{IV},j}\} \tag{25}$$

Thin Steel Plate

According to Eurocode 5 [39], a steel plate with a thickness smaller than half the dowel diameter is considered as thin steel plate. If a thin steel side plate is used, only Yield Mode II or $\mathrm{III_s}$ occurs. For Yield Mode II shown in Figure 18, lateral resistance can be obtained by treating $\alpha = \infty$ and $\beta = f_{\mathrm{h,CLT}}/f_{\mathrm{ha}} = 0$ in Equation (8), as follows.

$$R_{\mathrm{II},j} = cdf_{\mathrm{h,CLT}}\left(\sqrt{2 + \frac{4M_{\mathrm{II},j}}{c^2 d f_{\mathrm{h,CLT}}}} - 1\right) \tag{26}$$

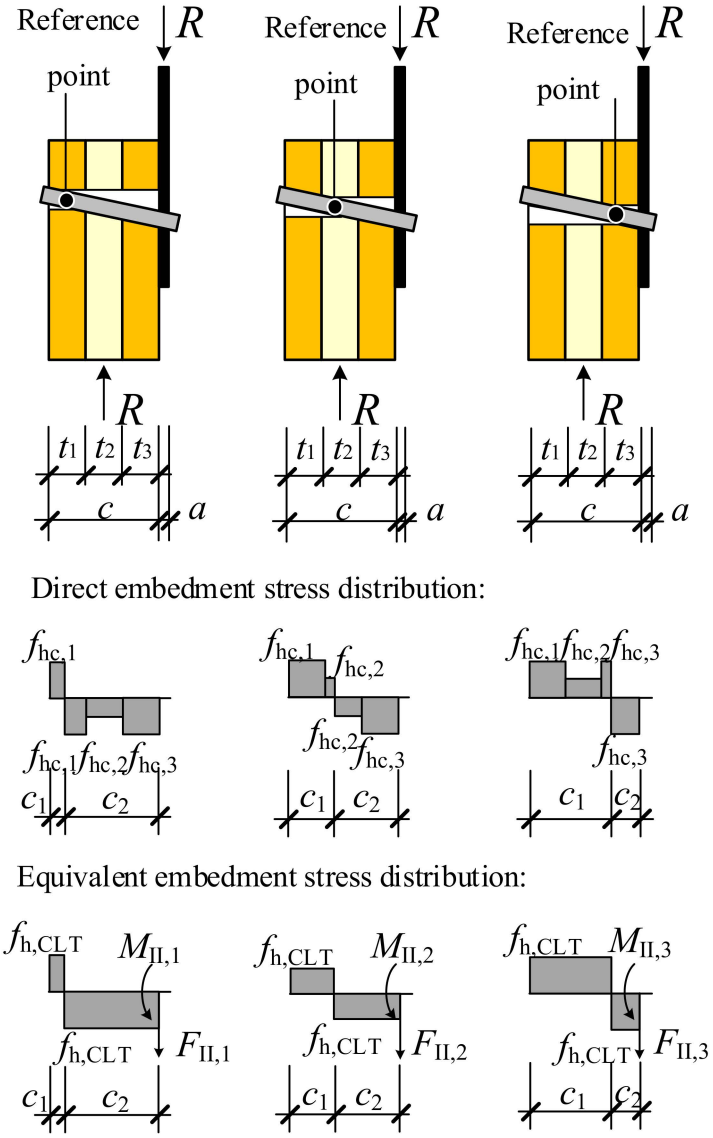


Figure 18. Embedment stress distribution for Yield Mode II (three-layer CLT).

For Yield Mode III$_s$ shown in Figure 19, a plastic hinge located in CLT is formed in the bolt, the lateral resistance can be obtained by treating $\alpha = \infty$ and $\beta = 0$ in Equation (16), as follows.

$$R_{\mathrm{IIIs},j} = \sqrt{2df_{\mathrm{h,CLT}}M_{\mathrm{y}} + 2df_{\mathrm{h,CLT}}M_{\mathrm{IIIs},j}} - F_{\mathrm{IIIs},j} \quad (27)$$

Lateral resistance of a steel-to-CLT connection with a thin steel side plate is smaller between Yield Modes II and III$_s$.

$$R = \min\{R_{\mathrm{II},j}, R_{\mathrm{IIIs},j}\} \quad (28)$$

For connections with a steel side plate falling between a thin and thick plate, the lateral resistance can be calculated by linear interpolation between the two situations [39].

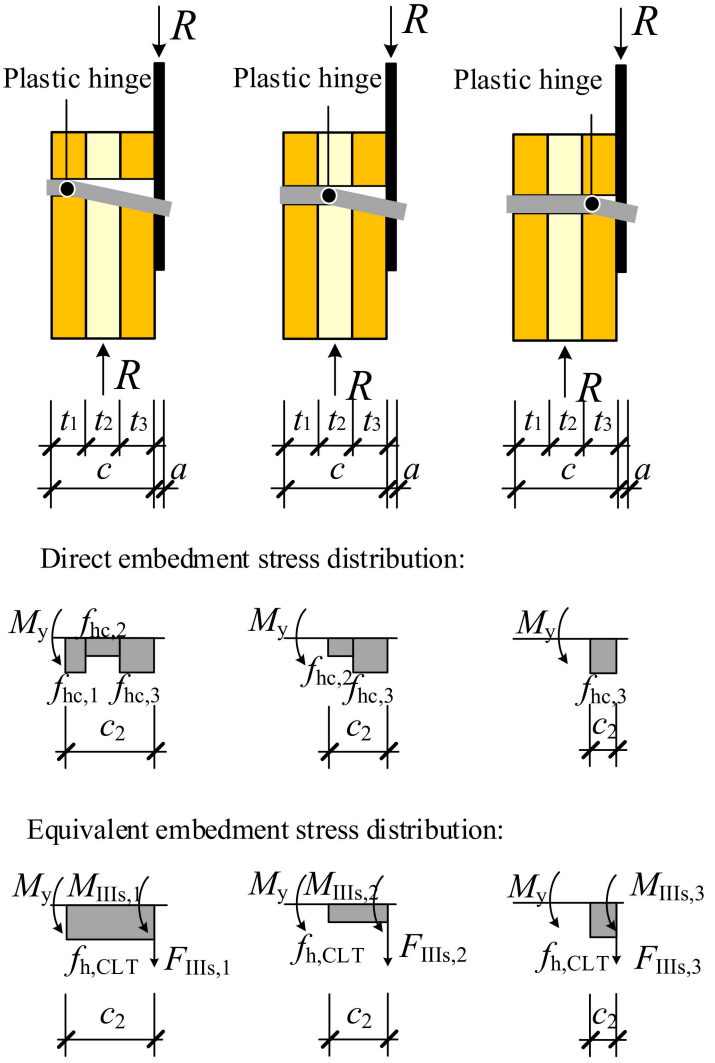


Figure 19. Embedment stress distribution for Yield Mode III_s (three-layer CLT).

3. Results

3.1. Material Properties

3.1.1. Yield Strength of Fasteners

Figure 20a shows the stress–strain curves of the bolts with a diameter of 12 mm, which present obvious yield and linear hardening behavior. The averaged yield strength of the bolts was 650 N/mm^2, 631 N/mm^2 and 626 N/mm^2, corresponding to diameters of 12 mm, 14 mm and 16 mm, respectively. As shown in Figure 20b, the screws exhibited high strength and nonlinear hardening behavior; hence the use of the nominal yield strength in this study, which corresponded to the 0.2% plastic strain. The averaged nominal yield strength of the self-tapping screws was 1509 N/mm^2 and 764 N/mm^2, corresponding to diameters of 5 mm and 10 mm, respectively. The yield bending moment of the bolts and screws can then be calculated with Equation (29).

$$M_y = \frac{k_w f_y \pi d^3}{32} \tag{29}$$

where k_w is the plastic coefficient, k_w = 1.4 according to Zhu [40], to reflect insufficient development of plasticity of bolt or screw; f_y is the yield strength of the bolt or screw.

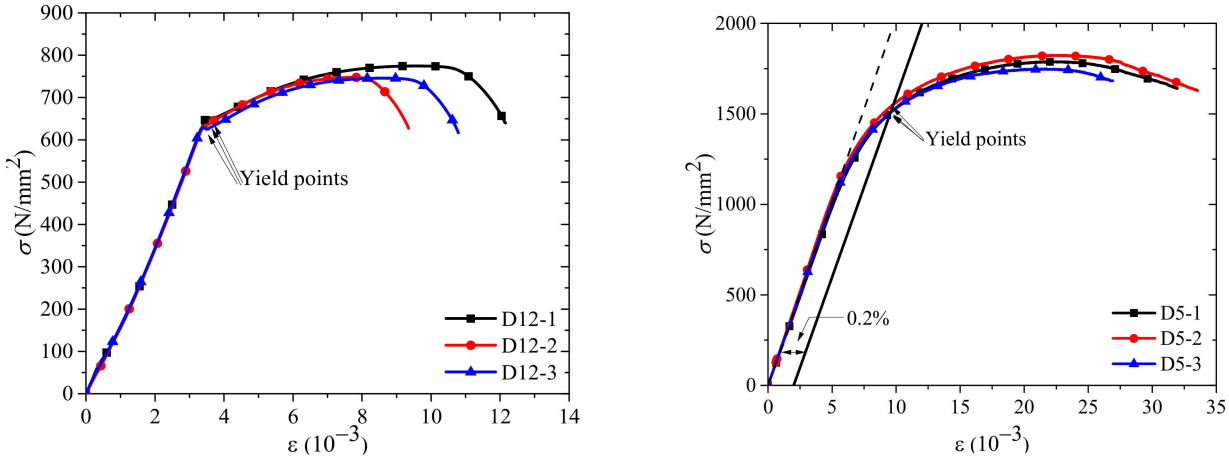


Figure 20. Stress–strain curves of the fasteners. (**a**) Bolts (d = 12 mm) and (**b**) screws (d = 5 mm).

3.1.2. Embedment Strength

The embedment strength, specific gravity and the moisture content of the CLT lamination specimens are listed in Table 4, together with the strength predicted with NDS [27]. Embedment strength of the CLT laminations from the test with the screw was all higher than the predicted value, whilst the embedment strength of the transversely loaded CLT laminations from the test with the bolt was lower than the prediction and the embedment strength of the longitudinally loaded laminations correlated with the prediction well. According to the test results of the bolted connections in Groups B1, B2, B3, B10, B11 and B12, the embedment strength of the Scotch Pine sawn lumber was 35.81 N/mm^2, 35.11 N/mm^2 and 39.52 N/mm^2, corresponding to the diameters of 12 mm, 14 mm and 16 mm, respectively. The averaged moisture content of the pine sawn lumber was 11.87%, and the averaged oven-dry specific gravity was 0.45.

Table 4. Test results of the embedment strength.

Grain Orientation	d (mm)	Embedment Strength f_h			Moisture Content		Oven-Dry Specific Gravity S_d	
		Average (N/mm^2)	COV	Predictions with NDS (N/mm^2)	Average (%)	COV	Average (%)	COV
Parallel	5	45.26	21.56	25.28	11.72	11.59	0.44	13.18
	10	40.18	21.32	34.65	11.88	13.86	0.45	11.56
	12	35.51	17.46	33.88	11.18	7.35	0.44	16.98
	14	27.03	18.14	30.03	12.19	17.46	0.39	12.69
	16	32.38	17.68	33.11	11.54	12.94	0.43	17.69
Perpendicular	5	32.34	29.17	24.23	11.46	9.04	0.43	11.60
	10	22.73	29.10	19.72	11.54	12.21	0.43	19.06
	12	14.75	31.84	18.00	11.25	5.50	0.43	15.77
	14	11.11	35.11	14.46	12.20	24.46	0.39	16.36
	16	11.16	32.96	14.55	11.65	13.45	0.41	16.42

3.2. Test Results of the Bolted Timber-to-CLT Connections

For all specimens, plasticity was well developed, and the yield mode of each connection was the same as that predicted by the proposed method. Specimens in Groups B1, B2, B3, B10, B11 and B12 developed into Yield Mode I$_s$, as the side members were all 10 mm thin. Specimens in Groups B4, B5, B6, B9, B13, B14 and B15 developed into Yield Mode III$_s$. Specimens in the rest groups developed into Yield Mode IV. The yield mode and the mean

yield load of specimens in each group calculated using the 5%*d* offset method are listed in Table 5.

Table 5. Results of the bolted timber-to-CLT connections.

Direction of Loading	Group	R_c [1] (kN)	$R_{c,EU}$ [2] (kN)	$R_{c,NDS}$ [3] (kN)	R_t [4] (kN)	Yield Mode	C_c [5]	$C_{c,EU}$ [6]	$C_{c,NDS}$ [7]
Longitudinal direction	B1	7.62	7.65	7.65	7.71	I_s	0.99	0.99	0.99
	B2	8.87	8.89	8.89	8.47	I_s	1.05	1.05	1.05
	B3	11.52	11.49	11.49	11.51	I_s	1.00	1.00	1.00
	B4	14.85	15.57	13.94	14.62	III_s	1.02	1.07	0.95
	B5	17.58	19.20	15.09	16.81	III_s	1.05	1.14	0.90
	B6	24.24	24.75	20.93	25.64	III_s	0.95	0.97	0.82
	B7	15.14	15.57	13.94	17.28	IV	0.88	0.90	0.81
	B8	23.31	19.20	15.09	25.38	IV	0.92	0.76	0.59
	B9	32.80	24.75	20.93	30.38	III_s	1.08	0.81	0.69
Transverse direction	B10	7.62	7.65	7.65	7.53	I_s	1.01	1.02	1.02
	B11	8.87	8.89	8.89	9.27	I_s	0.96	0.96	0.96
	B12	11.52	11.49	11.49	11.52	I_s	1.00	1.00	1.00
	B13	11.98	15.21	11.71	11.60	III_s	1.03	1.31	1.01
	B14	14.29	18.14	12.95	13.14	III_s	1.09	1.38	0.99
	B15	18.86	23.46	17.66	19.93	III_s	0.95	1.18	0.89
	B16	13.68	15.21	11.71	12.85	IV	1.06	1.18	0.91
	B17	17.33	18.14	12.95	16.12	IV	1.08	1.13	0.80
	B18	23.42	23.46	17.66	23.27	IV	1.01	1.01	0.76

[1] R_c is the lateral resistance calculated with the equations proposed in this study; [2] $R_{c,EU}$ is the lateral resistance calculated with the equations proposed by Uibel and Blaß [19,20]; [3] $R_{c,NDS}$ is the lateral resistance calculated with the equations stipulated in NDS-2018 [27]; [4] R_t is the lateral resistance from the test; [5] C_c is the verification coefficient, which is the ratio of the calculated lateral resistance to the test result, $C_c = R_c/R_t$; [6] $C_{c,EU}$ is the verification coefficient of the equations proposed by Uibel and Blaß [19,20], $C_{c,EU} = R_{c,EU}/R_t$; [7] $C_{c,NDS}$ is the verification coefficient of the equations stipulated in NDS-2018 [27], $C_{c,NDS} = R_{c,NDS}/R_t$.

3.2.1. Groups B1, B2, B3, B10, B11 and B12

Specimens in these groups behaved similarly and those in Group B10 are taken as an example to illustrate the test observations. The load–displacement curves of the specimens are shown in Figure 21a, all presenting an initial linear stage followed by a non-linear stage of the curves. As shown in Figure 22a for Specimen B10-1, Yield Mode I_s was observed, in which the bolt remained straight, and the wood of the side members yielded. The yield load of specimens in the six groups, ranging from 7.53 kN to 11.52 kN, was all due to yield of wood under the embedment stress. The difference in the yield load was mainly due to the difference in bolt diameter and variation of the embedment strength.

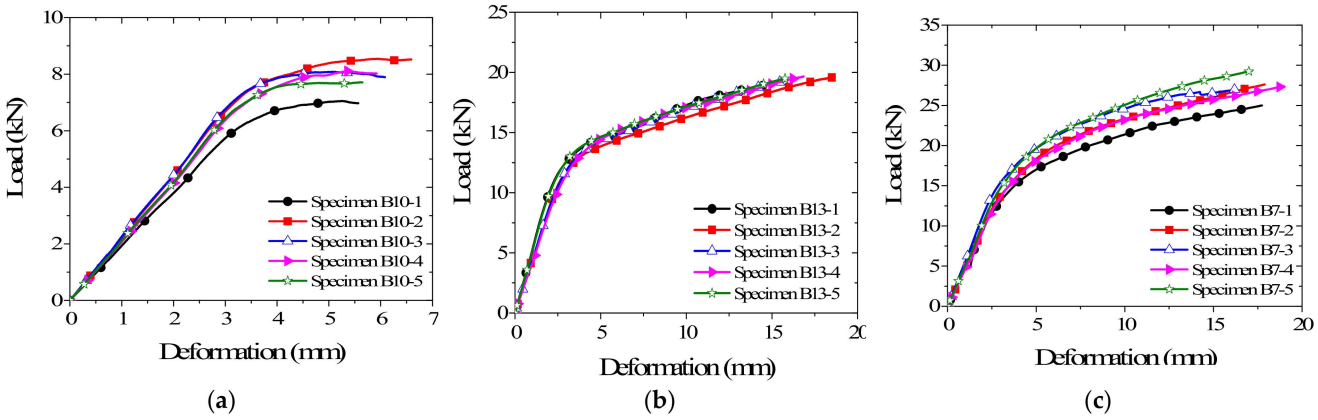
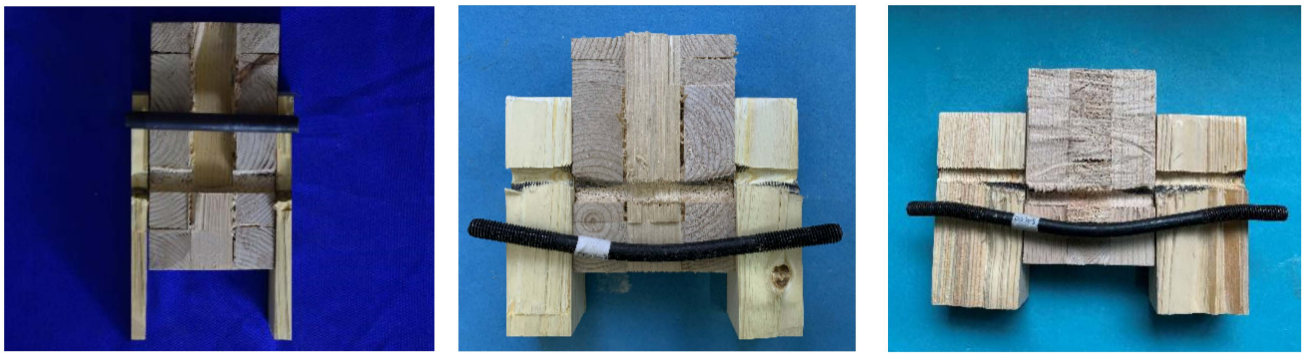


Figure 21. Load–displacement curves of bolted timber-to-CLT connections (d = 12 mm): (**a**) Group B10: Yield Mode I_s; (**b**) Group B13: Yield Mode III_s; and (**c**) Group B7: Yield Mode IV.



(**a**) (**b**) (**c**)

Figure 22. Typical yield mode of bolted timber-to-CLT connection specimens (d = 12 mm): (**a**) Specimen B10-1: Yield Mode I_s; (**b**) Specimen B13-1: Yield Mode III_s; and (**c**) Specimen B7-1: Yield Mode IV.

3.2.2. Groups B4, B5, B6, B9, B13, B14 and B15

Specimens in these groups also behaved similarly. Figure 21b shows the load–displacement curves of the specimens in Group B13, which present two-stage behavior that is obviously divided by a yield point. As shown in Figure 22b for the yield mode of Specimen B13-1, the bolt remained straight in the side member and bent in the CLT member, and two plastic hinges of the bolt were formed in the CLT member (one hinge to each shear plane), representing Yield Mode III_s. Due to thicker side members and yield of the bolt, higher lateral resistance and better plasticity were observed with specimens in these groups in comparison with the specimens that developed Yield Mode I_s.

3.2.3. Groups B7, B8, B16, B17 and B18

Figure 21c shows the load–displacement curves of specimens in Group B7, giving the highest lateral resistance since the side members were thick enough to accommodate one more plastic hinge. As shown in Figure 22c for the yield mode of Specimen B7-1, a plastic hinge of bolt was formed in both the CLT and the side members, confirming Yield Mode IV and good plasticity.

3.3. Test Results of the Screwed Steel-to-CLT Connections

As listed in Table 6, the yield mode of each specimen was the same as that predicted by the proposed method. Specimens with a 4 mm thick steel side plate developed into Yield Mode III_s, except for those in Group S6 that developed into Yield Mode II. For specimens with a 6 mm thick steel side plate, those in Group S8 developed into Yield Mode II, those in Group S4 developed into Yield Mode III_s and those in Groups S3 and S7 all developed into Yield Mode IV.

Table 6. The results of the single shear screwed steel-to-CLT connections.

Direction of Loading	Group	R_c (kN)	$R_{c,EU}$ (kN)	$R_{c,NDS}$ (kN)	R_t (kN)	Yield Mode	C_c	$C_{c,EU}$	$C_{c,NDS}$
Longitudinal direction	S1	4.55	6.97	4.04	3.81	I_s	1.19	1.83	1.06
	S2	9.19	13.21	8.41	9.74	I_s	0.94	1.36	0.86
	S3	5.52	7.89	4.58	5.40	I_s	1.02	1.46	0.85
	S4	9.95	14.31	9.11	10.55	III_s	0.94	1.36	0.86
Transverse direction	S5	4.19	6.97	3.87	3.39	I_s	1.24	2.06	1.14
	S6	3.56	13.21	7.84	3.86	IV	0.92	3.42	2.03
	S7	4.02	7.89	4.39	3.85	IV	1.04	2.05	1.14
	S8	4.15	14.31	8.48	4.07	IV	1.02	3.52	2.08

3.3.1. Groups S6 and S8

Specimens in these two groups behaved similarly to develop into Yield Mode II. It can be seen from the load–displacement curves of specimens in Group S8 shown in Figure 23a that the yield of the screwed connections was not obvious, and the plasticity was poor. This was due to the fact that the bolt hole was in non-uniform compression, the yield was local and the screw did not yield, just rotated as a rigid body in the connection, as shown in Figure 24a.

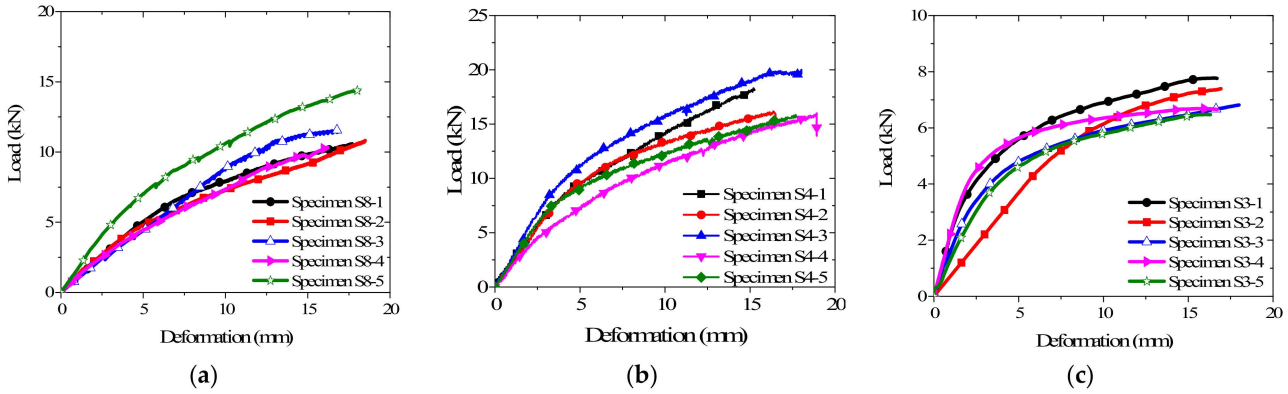


Figure 23. Load–displacement curves of screwed connection specimens: (**a**) Group S8: Yield Mode II; (**b**) Group S4: Yield Mode III_s; and (**c**) Group S3: Yield Mode IV.

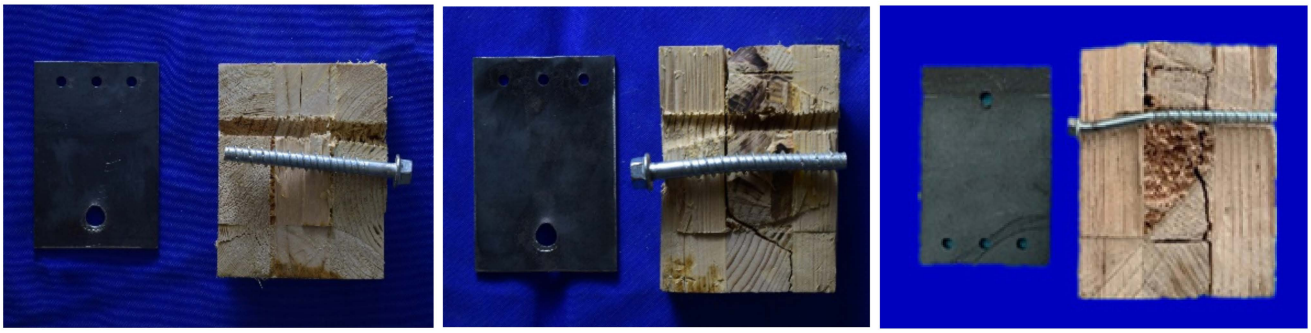


Figure 24. Typical yield modes of screwed steel-to-CLT connection specimens: (**a**) Specimen S8-1: Yield Mode II; (**b**) Specimen S4-1: Yield Mode III_s; and (**c**) Specimen S3-1: Yield Mode IV.

3.3.2. Groups S1, S2, S4 and S5

The screw diameter was larger than the thickness of the steel plate of the specimens in these groups, the clamping effect of the steel plate on the screw was weak and that of the CLT member on the screw was strong, and specimens in these groups all developed into Yield Mode III_s. The load–displacement curves of specimens in Group S4 are shown in Figure 23b, and the yield mode of Specimen S4-1 is shown in Figure 24b. The screw was thinner than a bolt and the strength of screw was much higher, so it was curved in the CLT member due to the small diameter (low stiffness) and only yielded nominally under high stress. As a result, the plasticity of these connections was less significant than the corresponding bolted connections that also developed into Yield Mode III_s.

3.3.3. Groups S3 and S7

In these groups, the thickness of the steel plate was larger than the screw diameter, and specimens all developed into Yield Mode IV. The load–displacement curves of specimens in Group S3 are shown in Figure 23c, and the yield mode of S3-1 is shown in Figure 24c, confirming Yield Mode IV as reflected by the two plastic hinges in the screw. Due to the

sufficient clamping effect both of the thick steel plate and CLT member on the screw, a plastic hinge was formed at the interface of the connected members, the other was formed in the CLT member. As a result, the nonlinear behavior of these specimens was more significant, and the yielding was more obvious with better plasticity compared with other screwed connections.

4. Discussion

For the bolted timber-to-CLT connections, the plasticity of the specimens that developed Yield Mode III_s or IV was better and the yield load was higher in comparison with the specimens that developed Yield Mode I_s. This was because that the clamping effect on the bolt increased with the increasing thickness of the side members, the connections developed plasticity increasing from being with yield of only the wood in Yield Mode I_s to being with yield of both the wood and bolts in Yield Mode III_s or IV. The mean of the embedment strength of wood and the yield strength of bolt obtained from the material tests were substituted into Equations (1)–(5) and (8)–(22) to calculate the lateral resistance R_c, which is listed in Table 5. The verification coefficient C_c, which is the ratio of the calculated lateral resistance to the test result, is also listed in the table. The verification coefficient for each group of specimens was all around 1.0, indicating that the lateral resistance of the connections was well predicted with the proposed method. The predicted yield mode of each connection was also consistent with the test observations. The lateral resistance calculated using methods proposed by Uibel and Blaß [19,20] and NDS-2018 [27] are also listed in Table 5, together with the corresponding verification coefficients. It can be seen that the proposed method in this study obtained significantly better accuracy overall.

Compared with the bolted timber-to-CLT connections, the load–displacement curves of the screwed connections in general did not show an obvious yield point, though significant nonlinear behavior was observed. The screws were made of carburized and quenched carbon steel, which were of high strength and poor plasticity. Due to the small diameter, the screw was clamped sufficiently by the CLT member, the bending stiffness of the screw was relatively small and the screw developed significant deflection. When the ultimate limit state controlled by deformation was reached, the wood yielded, but the screw yielded only nominally or even did not yield.

The 5%d offset method may not estimate the yield load of the screwed connections correctly where the plasticity is not well developed. Treating the wood as nonlinear foundation of the nail, Foschi [41] proposed a three-parameter exponential function model describing the behavior of laterally loaded nailed connections, which are similar to the screwed connections in terms of the strength and the geometrical dimension of the fasteners. The yield load is defined as the intersection of the initial elastic line of the load–slip curve and the asymptote of the curve as the slip tends to the infinity, as shown in Figure 25 [42].

Foschi's yield model was used to define the yield load of the screwed connections from the load–displacement curves obtained from the test in this study. The average yield load of the screwed connection specimens in each group is listed in Table 6. The yield loads determined with Foschi's yield model were all close to the analytical predictions following the EYM, with a verification coefficient C_c for each group of specimens around 1.0, as listed in the table. Foschi's yield model was consistent with the analytical predictions. The lateral resistance calculated using the methods proposed by Uibel and Blaß [19,20] and the methods in NDS-2018 [27] is also listed in Table 6, together with the corresponding verification coefficient. It can be seen that predictions by these two methods can deviate significantly from the test results owing to incorrect treatment of the embedment strength of CLT.

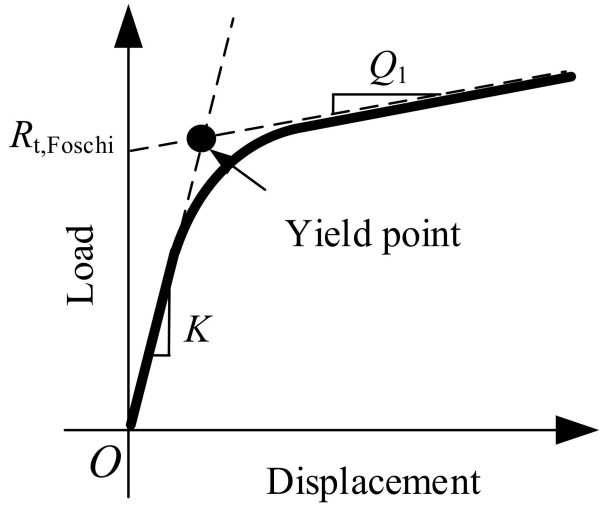


Figure 25. Foschi's yield model.

5. Conclusions

The effect of parameters like strength and diameter of bolt or screw and thickness of wood member or steel side plate on the yield mode, yield load and plasticity of the dowel-type connections was revealed experimentally in this study. Equations for predicting the lateral resistance and yield mode of the bolted and screwed connections of CLT by introducing the simplified equivalent embedment stress distribution were developed. Conclusions can be drawn as follows:

(1) The tests conducted in this study showed that the structural performance of the bolted connections of CLT can be different from that of the screwed connections, and the former develop better plasticity than the latter, due to the higher strength and more significant strain-hardening behavior of the screws, hence the different definitions of the yield load between the bolted and screwed connections.
(2) Compared with the test results, the accuracy of the proposed analytical method and the equations for predicting the lateral resistance of the bolted and screwed connections of CLT was significantly enhanced by introducing the simplified equivalent embedment stress distribution.
(3) The predicted lateral resistance and yield mode of the bolted and screwed connections of CLT using the proposed equations were consistent with the test results, and the correctness and the feasibility of the proposed analytical method and the equations were thus validated.

Author Contributions: Conceptualization, L.H. and E.Z.; methodology, E.Z.; software, G.W.; validation, L.H., S.N. and G.W.; formal analysis, L.H.; investigation, S.N.; resources, G.W.; data curation, S.N.; writing—original draft preparation, L.H.; writing—review and editing, E.Z.; visualization, L.H.; supervision, S.N.; project administration, E.Z.; funding acquisition, E.Z. All authors have read and agreed to the published version of the manuscript.

Funding: This research was funded by National Natural Science Foundation of China, grant number 51778187.

Institutional Review Board Statement: Not applicable.

Informed Consent Statement: Not applicable.

Data Availability Statement: All the data are contained within this article.

Acknowledgments: The authors acknowledge the advice and help offered by the members of Wood Structure Research Center, Harbin Institute of Technology.

Conflicts of Interest: The authors declare no conflict in the complete research.

References

1. Migda, W.; Szczepański, M.; Lasowicz, N.; Jakubczyk-Gałczyńska, A.; Jankowski, R. Non-linear analysis of Inter-Story Pounding between Wood-Framed Buildings during Ground Motion. *Geosciences* **2019**, *9*, 488. [CrossRef]
2. Johanides, M.; Kubíncová, L.; Mikolášek, D.; Lokaj, A.; Sucharda, O.; Mynarčík, P. Analysis of Rotational Stiffness of the Timber Frame Connection. *Sustainability* **2021**, *13*, 156. [CrossRef]
3. Gagnon, S.; Pirvu, C. *CLT Handbook: Crosslaminated Timber (Canadian Edition)*; FPInnovations: Quebec, QC, Canada, 2019.
4. Niederwestberg, J.; Zhou, J.; Chui, Y.H. Comparison of theoretical and laboratory out-of-plane shear stiffness values of cross laminated timber panels. *Buildings* **2018**, *8*, 146. [CrossRef]
5. Sandoli, A.; Calderoni, B. The Rolling Shear Influence on the Out-of-Plane Behavior of CLT Panels: A Comparative Analysis. *Buildings* **2020**, *10*, 42. [CrossRef]
6. Wu, G.; Zhong, Y.; Ren, H. Effects of Grain Pattern on the Rolling Shear Properties of Wood in Cross-Laminated Timber. *Forests* **2021**, *12*, 668. [CrossRef]
7. Huo, L.; Wu, G.; Wang, H.; Zhu, E. Calculation of stability coefficient of cross-laminated timber members in axial compression. *J. Build. Struct.* **2021**, *42*, 107–116. [CrossRef]
8. Ettelaei, A.; Taoum, A.; Shanks, J.; Nolan, G. Rolling Shear Properties of Cross-Laminated Timber Made from Australian Plantation *Eucalyptus nitens* under Planar Shear Test. *Forests* **2022**, *13*, 84. [CrossRef]
9. Casagrande, D.; Rossi, S.; Sartori, T.; Tomasi, R. Proposal of an analytical procedure and a simplified numerical model for elastic response of single-storey timber shear-walls. *Constr. Build. Mater.* **2016**, *102 Pt 2*, 1101–1112. [CrossRef]
10. Brandner, R.; Flatscher, G.; Ringhofer, A.; Schickhofer, G.; Thiel, A. Cross laminated timber (CLT): Overview and development. *Eur. J. Wood Wood Prod.* **2016**, *74*, 331–351. [CrossRef]
11. Pei, S.; Lindt, J.V.D.; Popovski, M.; Berman, J.W.; Dolan, J.D.; Ricles, J.; Sause, R.; Blomgren, H.; Rammer, D.R. Cross-laminated timber for seismic regions: Progress and challenges for research and implementation. *J. Struct. Eng.* **2016**, *142*, E2514001. [CrossRef]
12. Ceccotti, A. New technologies for construction of medium-rise buildings in seismic regions: The XLAM case. *Struct. Eng. Int.* **2008**, *18*, 156–165. [CrossRef]
13. Ceccotti, A.; Sandhaas, C.; Okabe, M.; Yasumura, M.; Minowa, C.; Kawai, N. SOFIE project—3D shaking table test on a seven-storey full-scale cross-laminated timber building. *Earthq. Eng. Struct. Dyn.* **2013**, *42*, 2003–2021. [CrossRef]
14. Johansen, K.W. Theory of timber connections. *Int. Assoc. Bridge Struct. Eng.* **1949**, *9*, 249–262. [CrossRef]
15. Wilkinson, T.L. *Dowel Bearing Strength*; FPL-RP-505; Forest Products Laboratory: Madison, WI, USA, 1991.
16. Ehlbeck, J.; Werner, H. Softwood and hardwood embedding strength for dowel-type fasteners. In Proceedings of the 25th Meeting of the Working Commission W18-Timber Structures, International Council for Building Research Studies and Documentation (CIB/W18), Ahus, Sweden, 24–27 August 1992.
17. Whale, L.R.J.; Smith, I.; Larsen, H.J. Design of nailed and bolted joints proposals for the revision of existing formulae in draft Eurocode 5 and CIB code. In Proceedings of the 20th Meeting of the Working Commission W18-Timber Structures, International Council for Building Research Studies and Documentation (CIB/W18), Dublin, Ireland, September 1987; International Council for Research and Innovation in Building and Construction: Rotterdam, The Netherlands, 1987.
18. Ringhofer, A.; Brandner, R.; Blaß, H.J. Cross-laminated timber (CLT): Design approaches for dowel-type fasteners and connections. *Eng. Struct.* **2018**, *171*, 849–861. [CrossRef]
19. Uibel, T.; Blaß, H.J. Load carrying capacity of joints with dowel type fasteners in solid wood panels. In Proceedings of the 39th Meeting of the Working Commission W18-Timber Structures, International Council for Building Research Studies and Documentation (CIB/W18), Florence, Italy, 28–31 August 2006.
20. Uibel, T.; Blaß, H.J. Edge joints with dowel type fasteners in cross-laminated timber. In Proceedings of the 40th Meeting of the Working Commission W18-Timber Structures, International Council for Building Research Studies and Documentation (CIB/W18), Bled, Slovenia, 28–31 August 2007.
21. Wallner-Novak, M.; Augustin, M.; Koppelhuber, J.; Pock, K. *Cross-Laminated Timber Structural Design Volume 2—Applications*; Proholz Austria: Vienna, Austria, 2018.
22. Gustafsson, A. *KL-Trahandbok*; Foreningen Sveriges Skogsindustrier: Skelleftea, Sweden, 2017. (In Swedish)
23. Tuhkanen, E.; Mölder, J.; Schickhofer, G. Influence of number of layers on embedment strength of dowel-type connections for glulam and cross-laminated timber. *Eng. Struct.* **2018**, *176*, 361–368. [CrossRef]
24. Muñoz, W.; Mohammad, M.; Gagnon, S. Lateral and withdrawal resistance of typical CLT connections. In Proceedings of the 11th world conference on timber engineering (WCTE 2010), Riva del Garda, Italy, 20–24 June 2010.
25. Kennedy, S.; Salenikovich, A.; Muñoz, W.; Mohammad, M. Design equations for dowel embedment strength and withdrawal resistance for threaded fasteners in CLT. In Proceedings of the 13th world conference on timber engineering (WCTE 2014), Quebec, QC, Canada, 10–14 August 2014.
26. *CSA O86–19*; Engineering Design in Wood. Canadian Standard Association: Mississauga, ON, Canada, 2019.
27. *ANSI/AWC NDS-2018*; National Design Specification for Wood Construction. American Wood Council: Washington, DC, USA, 2018.
28. Shoichi, N.; Akihisa, K.; Takuro, M.; Kohei, K. Propose alternative design criteria for dowel type joint with CLT. *RILEM Bookseries* **2014**, *9*, 739–748. [CrossRef]

29. Mahdavifar, V.; Sinha, A.; Barbosa, A.R.; Muszynski, L.; Gupta, R. Lateral and withdrawal capacity of fasteners on hybrid cross-laminated timber panels. *J. Mater. Civil Eng.* **2018**, *30*, 04018226. [CrossRef]
30. *GB 50017-2017*; Standard for Design of Steel Structures. China Architecture & Building Press: Beijing, China, 2017. (In Chinese)
31. *ASTM D 5764-97a (Reapproved 2013)*; Standard Test Methods for Evaluating Dowel-BEARING Strength of Wood and Wood-Based Products. ASTM: West Conshohocken, PA, USA, 2013.
32. *GB 50005-2017*; Standard for Design of Timber Structures. China Architecture & Building Press: Beijing, China, 2017. (In Chinese)
33. *ASTM D 5652-15*; Standard Test Methods for bolted CONNECTIONS in Wood and Wood-Based Products. ASTM: West Conshohocken, PA, USA, 2015.
34. *ASTM A 370-17*; Standard Test Methods and Definitions for Mechanical Testing of Steel Products. ASTM: West Conshohocken, PA, USA, 2017.
35. *ASTM F 606-16*; Standard Test Methods for Determining the Mechanical Properties of Externally and Internally Threaded Fasteners, Washers, Direct Tension Indicators, and Rivets. ASTM: West Conshohocken, PA, USA, 2016.
36. *ASTM D 2395-17*; Standard Test methods for Specific GRAVITY of Wood and Wood-Based Materials. ASTM: West Conshohocken, PA, USA, 2017.
37. *ASTM D 4442-20*; Standard Test Methods for Direct Moisture Content Measurement of Wood and Wood-Base Materials. ASTM: West Conshohocken, PA, USA, 2020.
38. Larsen, H.J.; Enjily, V. *Practical Design of Timber Structures to Eurocode 5*; Thomas Telford Limited: London, UK, 2009.
39. *EN 1995-1-1: 2004*; Eurocode 5: Design of Timber Structures—Part 1-1: General—Common Rules and Rules for Buildings. CEN: Brussels, Belgium, 2004.
40. Zhu, E.C.; Pan, J.L. *Probing into the Problems in Design of Wood Structures*; China Architecture & Building Press: Beijing, China, 2017. (In Chinese)
41. Foschi, R.O. Load-slip characteristic of nails. *Wood Sci.* **1974**, *7*, 69–76.
42. Jumaat, M.Z.; Murty, B. Yield load prediction of nailed timber joints using nail diameter and timber specific gravity. *Wood Sci. Technol.* **2004**, *38*, 599–615. [CrossRef]